Journal of Power Sources 187 (2009) 93–97

Contents lists available at ScienceDirect

Journal of Power Sources

journal homepage: www.elsevier.com/locate/jpowsour

Short communication

X-ray absorption analysis of nitrogen contribution to oxygen reduction reaction in carbon alloy cathode catalysts for polymer electrolyte fuel cells

Hideharu Niwa[a], Koji Horiba[a,b], Yoshihisa Harada[a,b], Masaharu Oshima[a,b,*], Takashi Ikeda[c], Kiyoyuki Terakura[d], Jun-ichi Ozaki[e], Seizo Miyata[f]

[a] Department of Applied Chemistry, The University of Tokyo, 7-3-1 Bunkyo-ku, Tokyo 113-8656, Japan
[b] The University of Tokyo Synchrotron Radiation Research Organization, 7-3-1 Bunkyo-ku, Tokyo 113-8656, Japan
[c] Quantum Beam Science Directorate, Japan Atomic Energy Agency (JAEA), Hyogo 679-5148, Japan
[d] Research Center for Integrated Science, Japan Advanced Institute of Science Technology (JAIST), 1-1 Asahidai, Nomi Ishikawa 923-1292, Japan
[e] Department of Chemical & Environmental Engineering, Graduate School of Engineering, Gunma University, 1-5-1 Tenjin-cho, Kiryu, Gunma 376-8515, Japan
[f] New Energy and Industrial Technology Development Organization, 1310 Omiya-cho, Saiwai-ku, Kawasaki, Kanagawa 212-8554, Japan

ARTICLE INFO

Article history:
Received 29 August 2008
Received in revised form 16 October 2008
Accepted 17 October 2008
Available online 25 October 2008

Keywords:
Polymer electrolyte fuel cell
Cathode
X-ray absorption spectroscopy
Carbon alloys

ABSTRACT

The electronic structure of nitrogen introduced into various carbon-based cathode catalysts for the polymer electrolyte fuel cell (PEFC) is investigated using X-ray absorption spectroscopy (XAS). The profile of π^* peaks at the pre-edge of N 1s XAS spectra is used to determine the chemical state of nitrogen, which can be an indicator of oxygen reduction reaction (ORR) activity. It is found that catalysts with a relatively larger amount of graphite-like nitrogen exhibit a higher ORR activity than those with a relatively larger amount of pyridine-like nitrogen. We propose that effective doping with graphite-like nitrogen is a practical guideline for the synthesis of active carbon alloy catalysts.

1. Introduction

Recently, fuel cells have attracted much attention as a clean energy storage system with the potential to resolve the world's energy problems. In particular, the polymer electrolyte fuel cell (PEFC) is expected to be a promising power source of high efficiency, low operating temperature, and low pollution for transportation and residential applications [1,2]. Considerable effort has been devoted to solving several problems associated with the use of fuel cell cathode electrocatalysts. Conventionally, Pt has been used as a cathode electrocatalyst for slow oxygen reduction reaction (ORR) [1]. However, as a precious metal, Pt is too expensive to use as a cathode catalyst [2]. Thus, to markedly reduce the cost of electrocatalysts, the use of Pt should be limited. To this goal, effective loading methods of Pt [3], Pt-alloys [4] and various non-Pt catalysts [5–14] have been developed. For the practical use of PEFCs, however, alternative low-cost non-Pt cathode catalysts with high power loads are necessary. Although most non-Pt catalysts contain metals, some carbon-based materials have been reported to show high ORR activities [9–14]. Among them, carbon-based materials doped with nitrogen and/or boron are receiving much attention owing to their relatively high ORR activities [9–12,14]. These materials, which are a mixture of carbon materials modified by inexpensive elements such as hydrogen, boron, and nitrogen, are called 'carbon alloys' [15].

There is much debate on the location of the active site in carbon alloys [16]. In general, carbon alloy catalysts are derived from carbon-based precursors containing transition metals such as Fe and Co. After pyrolysis of the precursors, the transition metals are removed by acid washing [11,13]. In this process, it is considered that an active site is produced in defects at the edge plane introduced into the surface of carbon alloys [13,16]. Moreover, transition metals still remaining after acid washing may work as an active site similarly to other organic macrocycles [5,6]. In fact, some carbon alloy catalysts with no transition metals in their precursors show ORR activities [9,10,13], experimentally confirming that carbon, nitrogen or another light element itself can be the active site. Quite recently, the role of nitrogen in carbon alloy catalysts

* Corresponding author. Tel.: +81 3 5841 7191; fax: +81 3 5841 8744.
E-mail address: oshima@sr.t.u-tokyo.ac.jp (M. Oshima).

0378-7753/$ – see front matter © 2008 Elsevier B.V. All rights reserved.
doi:10.1016/j.jpowsour.2008.10.064

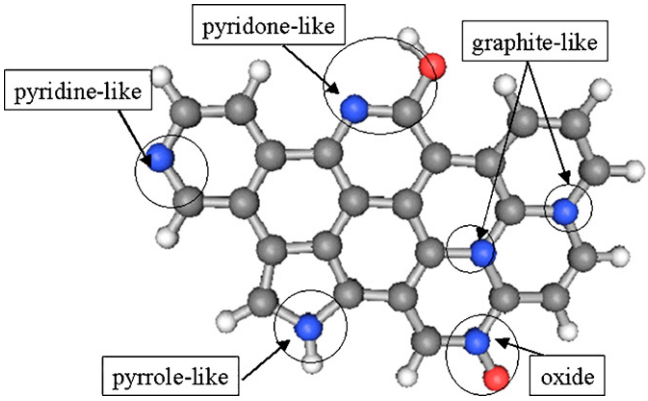

Fig. 1. Local geometry for various nitrogens in graphite. Gray, blue, red, and white balls represent carbon, nitrogen, oxygen, and hydrogen atoms, respectively. (For interpretation of the references to color in this figure legend, the reader is referred to the web version of the article.)

has attracted much attention since nitrogen doping enhances ORR activity [9–12,14]. Note that the relationship between the chemical state of nitrogen and the ORR activity of carbon alloy catalysts has long been a topic of debate. Maldonado and Stevenson [14] indicated that exposed edge plane defects and nitrogen doping are important factors for enhancing electrocatalysis for ORR. Matter et al. [13] hold that even though the most active catalyst has a significantly higher amount of pyridine-like nitrogen (Fig. 1), pyridine-like nitrogen itself may not be the active site for ORR, but may only be an indicator of edge plane exposure, on which many electrocatalytic reactions show increased kinetics. However, the role of the nitrogen in ORR activity remains to be elucidated. The term "edge plane" or "defects" that indicate the active site is somewhat ambiguous. In order to discuss the population of all nitrogen sites quantitatively and study the role of nitrogen in catalytic activity, we need information on the electronic states of nitrogen in carbon alloy catalysts. A few X-ray photoelectron spectroscopy (XPS) studies have determined the chemical state of doped nitrogen ions in carbon alloy catalysts [9,10,12–14]. However, there are as yet no studies on the valence electronic states of nitrogen, which should provide direct information on how doped nitrogen enhances or reduces ORR activity.

In this study, we directly investigated the valence electronic states of nitrogen in carbon alloys by soft X-ray absorption spectroscopy (XAS) to clarify the role of nitrogen in cathode catalyst activity and to develop more efficient catalysts.

2. Experimental

2.1. Sample preparation and characterization

We prepared three types of sample to identify the active site: (1) nanoshell carbon derived from pyrolyzed cobalt phthalocyanine and nitrogen-containing polymers followed by acid washing to remove cobalt (CoPc-ph-900); (2) nitrogen-doped carbon alloys (AO50 and AO90) prepared by ammo-oxidation, which is a means of doping nitrogen into carbon black with ammonia; and (3) nitrogen-doped carbon materials prepared by another method (N1 and N2) in which the precursors contain nitrogen atoms. Details of the preparation and the electrochemical characterization of N1 and N2 have been described elsewhere [9]. As shown in Table 1, we determined the composition ratios of nitrogen to carbon for CoPc-ph-900, N1, N2, AO50 and AO90 to be 0.008, 0.005, 0.021, 0.014 and 0.012, respectively, by means of hard X-ray photoemission spectroscopy, which is more bulk-sensitive than conventional XPS. Details have been described elsewhere [17]. Bulk sensitive hard X-ray photoemission spectroscopy of CoPc-ph-900 showed no Co within the detection limit. The content of Co is less than 0.04 at.% [17].

Table 1
Surface composition ratios of nitrogen to carbon by HXPES and activity for oxygen reduction reaction (ORR) measured by rotating disk electrode voltammetry. Onset potential E_{onset} is defined as the voltage where the reduction current density of $-10\,\mu A\,cm^{-2}$ is reached. Current density at 0.40 V vs. NHE is also described. The specific current density $i_{0.4\,BET}$ is normalized current density by the BET surface areas of the carbon alloys at 0.4 V vs. NHE.

Sample	N/C	E_{onset} (vs. NHE)	$i_{0.4}$ (mA cm^{-2})	$i_{0.4\,BET}$ (mA m^{-2} BET)
AO50	0.014	0.58 V	−0.12	−0.5
AO90	0.012	0.57 V	−0.07	−0.3
N1	0.005	0.45 V	−0.03	−0.4
N2	0.021	0.45 V	−0.03	−1.2
CoPc-ph-900	0.008	0.74 V	−0.30	−4.0

ORR activity was evaluated by rotating disk voltammetry in 0.5 mol l^{-1} H_2SO_4 saturated with oxygen at room temperature [9].

2.2. XAS measurements and calculation

XAS was carried out at the BL-2C of the Photon Factory of the High Energy Accelerator Research Organization (KEK). This beamline has a U02 undulator and a grazing incidence monochromator to provide high-resolution soft X-rays ($E/\Delta E < 10000$). For XAS measurements, the samples were synthesized in air and transferred to an ultrahigh-vacuum chamber (base pressure $\sim 4.0 \times 10^{-10}$ Torr) at room temperature. XAS spectra were recorded in the total electron yield (TEY) mode by measuring the sample current and then normalized to the mirror current. Incident photon energy was changed from 395 eV to 440 eV to measure the absorption spectra over the N 1s absorption edge at around 400 eV.

Calculations were carried out using the restrict Hartree Fock (RHF) theory in the GAMESS program [18]. We model the carbon alloy catalysts using nitrogen-doped heterocyclic molecular models. We use the HF/3-21G *ab initio* molecular orbital method to optimize the geometries of the molecular models and calculate the energies of the optimized structures. The energy of the X-ray absorption peaks are estimated from the difference between the nitrogen core level and the unoccupied π^* orbital energy.

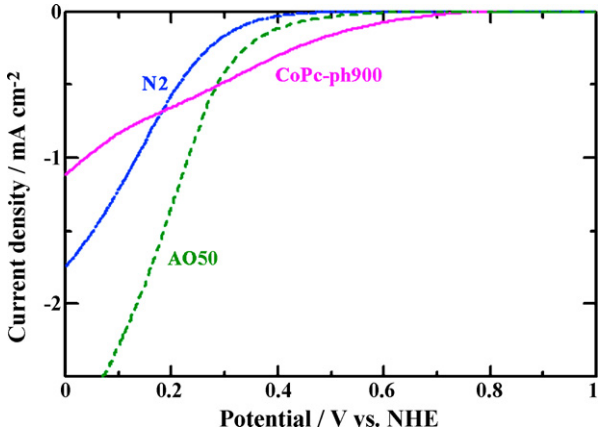

Fig. 2. Voltammogram of ORR on AO50, N2 and CoPc-ph-900.

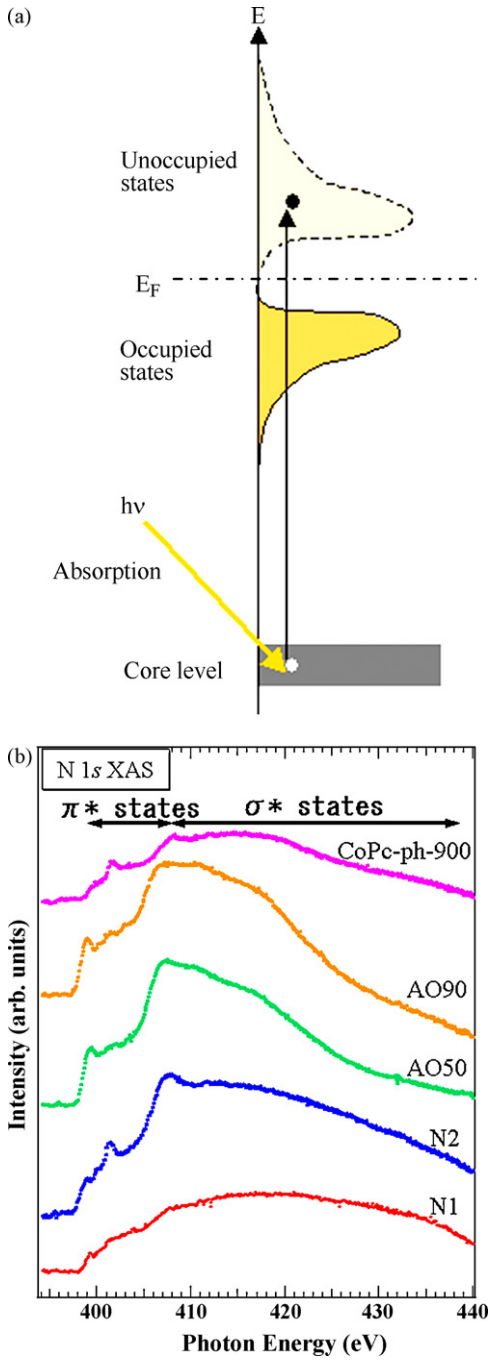

Fig. 3. (a) The schematic for X-ray absorption. (b) Nitrogen 1s XAS spectra for carbon alloy catalysts.

3. Results and discussion

3.1. ORR activities and surface nitrogen contents of carbon alloy catalysts

The ORR activities are summarized in Table 1 and Fig. 2. All the samples show reduction currents with a negative sweep of the potential. AO50 and AO90, which have similar nitrogen contents, show similar ORR activities, whereas N2, which contains more nitrogen than N1, shows much higher ORR activities in terms of the specific current density $i_{0.4\,\mathrm{BET}}$ [9]. Unlike noble metal catalyst, the current density of N1 or N2 at 0.9 V vs. NHE is so small that we employed the current density at 0.4 V vs. NHE as an indicator of ORR activity. Among all the samples, CoPc-ph-900 shows the highest ORR activity despite having the lowest nitrogen content, suggesting that nitrogen in CoPc-ph-900 are most efficiently incorporated into ORR active sites.

3.2. XAS analysis

Fig. 3 shows the principle of XAS and the N 1s XAS spectra of CoPc-ph-900, N1, N2, AO50, and AO90. X-ray absorption is resonantly enhanced when the N 1s core electron is excited to unoccupied π^* or σ^* states. Across the absorption edge, the transition from the N 1s core level to the antibonding π^* molecular orbital occurs. Above the ionization potential energy, the transition to the antibonding σ^* orbital is predominant. The XAS spectra have mainly three prominent peaks in the $1s \rightarrow \pi^*$ region and a broad feature centered at ~407 eV in the $1s \rightarrow \sigma^*$ region, as shown in Fig. 3(b).

In the σ^* region, we can estimate the C–N bond length R using the following empirical equation proposed by Ripalda et al. [19], which is expressed as a function of the σ^* resonance energy Δ_σ defined by the energy difference between the σ^* peak energy and the ionization potential:

$$R = 0.148\ \mathrm{nm} - (0.00243\ \mathrm{nm\,eV^{-1}})\,\Delta_\sigma. \quad (1)$$

This is an interpolation of the experimental data for small molecules collected by Stöhr [20]. The rough estimation of the C–N bond length obtained by applying the above equation to our XAS data indicates the existence of sp^2 hybridized C–N bonds whose expected bond lengths range from 1.40 Å (three carbon neighbors) to 1.33 Å (two carbon neighbors), and the absence of sp and sp^3 hybridized C–N bonds whose expected bond lengths are 1.16 Å and 1.47 Å, respectively. The σ^* peak energies and estimated bond lengths of the carbon alloy catalysts are shown in Table 2. The uncertainty margin in these bond lengths is due to the uncertainty in the determination of ionization potential.

In the $1s \rightarrow \pi^*$ region, two prominent peaks (A1 and A3) and one small peak (A2) are observed, as shown in Fig. 4(a). Many studies have assigned π^* peaks to different C–N bonds. Mubumbila et al. [21] assigned A1 to constrained C–N bonds, A2 to pyridine-like double bonds, and A3 to nitrogen atoms inside graphite domains.

Another interpretation is as follows: the A1 at ~399.1 eV is assigned to an sp^2 hybridized pyridine-like nitrogen that has two carbon neighbors with a double bond C=N; the A3 at ~401.5 eV is

Table 2
Peak positions of nitrogen 1s XAS and expected C–N bond length.

Samples	Absorption edge (eV)	Peak A1 (eV)	Peak A2 (eV)	Peak A3 (eV)	σ^* peak (eV)	Expected C–N bond length (nm)
AO50	397.8	399.4	400.4	401.9	407.5	1.40 ± 0.10
AO90	397.5	398.9	400.2	401.4	407.1	1.40 ± 0.10
N1	398	399.2	–	401.3	407.7	1.39 ± 0.10
N2	397.5	398.9	400	401.4	407.7	1.39 ± 0.10
CoPc-ph-900	398.8	–	399.7	401.4	408.2	1.38 ± 0.10

Table 3a
Calculated X-ray absorption energies for molecular models which have pyridine-like nitrogen.

Molecular model	X-ray absorption energy (eV)	Molecular formula
PL1	424.15	C_9H_7N
PL2	423.90	C_9H_7N
PL3	424.10	$C_{15}H_9N$
PL4	423.00	$C_{15}H_9N$
PL5	424.05	$C_{11}H_8N_2$
PL6	424.00	$C_{11}H_8N_2$
PL7	423.99	$C_7H_6N_2$
PL8	423.85	$C_{13}H_9N$
Average	423.88	

Table 3b
Calculated X-ray absorption energies for molecular models which have graphite-like nitrogen.

Molecular model	X-ray absorption energy (eV)	Molecular formula
GL1	426.45	$C_{12}H_9N$
GL2	426.90	$C_{10}H_7N$
GL3	426.25	$C_{18}H_9N$
GL4	427.39	$C_{12}H_9N$
GL5	426.75	$C_{11}H_8N_2$
GL6	426.65	$C_{11}H_8N_2$
GL7	426.45	$C_{12}H_{10}N_2$
GL8	425.90	$C_{12}H_{10}N_2$
Average	426.59	

assigned to an sp^2 hybridized graphite-like nitrogen that has three carbon neighbors; and the A2 at ~400.1 eV is assigned to a cyanide-like nitrogen that has a triple bond [16,22,23]. The peak energies of the carbon alloy catalysts in the $1s \rightarrow \pi^*$ region are listed in Table 2.

We calculated nitrogen $1s \rightarrow \pi^*$ transition energy using the GAMESS program assuming 16 structural models, half of which have pyridine-like nitrogen and the other half have graphite-like nitrogen. Details of the molecular models are shown in Tables 3a and 3b. The calculated nitrogen $1s \rightarrow \pi^*$ transition energies are plotted in Fig. 4(b). They are split into two regions according to the models, i.e., pyridine-like nitrogens with blue circles and graphite-like nitrogens with red squares. The *x*- and *y*-axes denote the N $1s \rightarrow \pi^*$ transition energy and the N 1s binding energy averaged among the pyridine-like nitrogens, respectively. On the basis of the π^* peaks in the experiment, we assigned the blue circles to A1 and the red squares to A3. The energy difference Δ between the N $1s \rightarrow \pi^*$ transition energies averaged within A1 and A3 is approximately 2.7 eV, which coincides with the experimental data in Fig. 4(a).

To correlate the chemical state of nitrogen with ORR activity, all the XAS spectra are compared in Fig. 5. The XAS spectra are normalized by an integrated π^* intensity from 396 eV to 404 eV which well represents the sum of electronic contribution of nitrogen sites to the π^* states. As shown in Fig. 5(a), AO50 and AO90 with very similar ORR activities have similar XAS profiles in the π^* region consisting of the main peak A1 (pyridine-like) and the small peak A3 (graphite-like), despite their difference in A1 intensity and small difference at A2 (cyanide-like nitrogen). As shown in Fig. 5(b), N2, which contains more nitrogen than N1, shows increased intensities around A1 (pyridine-like nitrogen), A2 (cyanide-like nitrogen) and A3 (graphite-like nitrogen). Since the difference at A1 and small difference at A2 are also seen in Fig. 5(a), it should be noted that the difference at A3 is more important. It is notable that N2, which shows higher ORR activity than N1, contains more graphite-like nitrogen. Fig. 5(c) shows the difference between CoPc-ph-900 and N2. There is no significant difference at A2 (cyanide-like nitrogen)

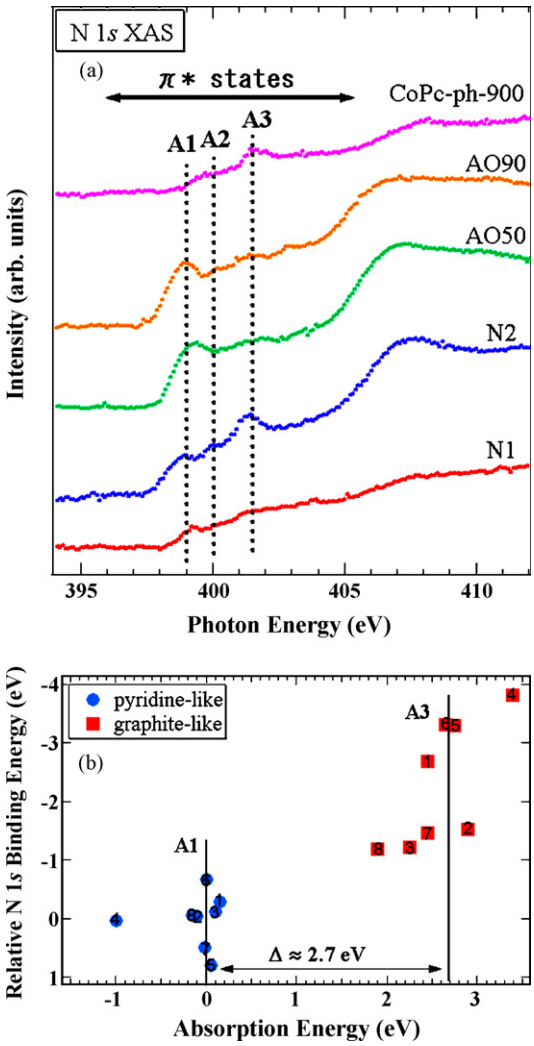

Fig. 4. (a) XAS N $1s \rightarrow \pi^*$ spectra for carbon alloy catalysts and (b) calculated relative N 1s binging energies and relative X-ray absorption energies for graphite-like (A3) and pyridine-like (A1) nitrogen atoms in graphene. Numbers in Fig. 3(b) correspond to the molecular models in Tables 3a and 3b.

compared to A1 and A3. At A1 (pyridine-like nitrogen), CoPc-ph-900 shows a much lower intensity than N2. However, from the above discussion, the pyridine-like nitrogen does not seem to increase ORR activity. CoPc-ph-900, which exhibits the highest ORR activity, shows a higher intensity at peak A3 (graphite-like nitrogen) than N2. Thus, we conclude that higher ORR-activity catalysts contain a larger amount of graphite-like nitrogen than of other types of nitrogen. Thus, we assume that the π^* profile, which reflects the local geometrical information, can be an indicator of ORR activity.

The above results also show that the bonding state of the doped nitrogen differs depending on the catalyst preparation method. AO50 and AO90, whose were nitrogen was doped with ammonia, contain a large amount of pyridine-like nitrogen. Therefore, nitrogen introduced by this ammo-oxidation method is likely to be introduced as pyridine-like nitrogen. On the other hand, carbon alloys synthesized by the pyrolysis of nitrogen-containing precursors, such as CoPc-ph-900, N1 and N2, contain a large amount of graphite-like nitrogen. Therefore, it is expected that if we can introduce graphite-like nitrogen effectively, more active carbon alloy catalysts can be synthesized.

A recent molecular dynamics simulation showed that carbon atoms bonded to graphite-like nitrogen at only the zigzag edge

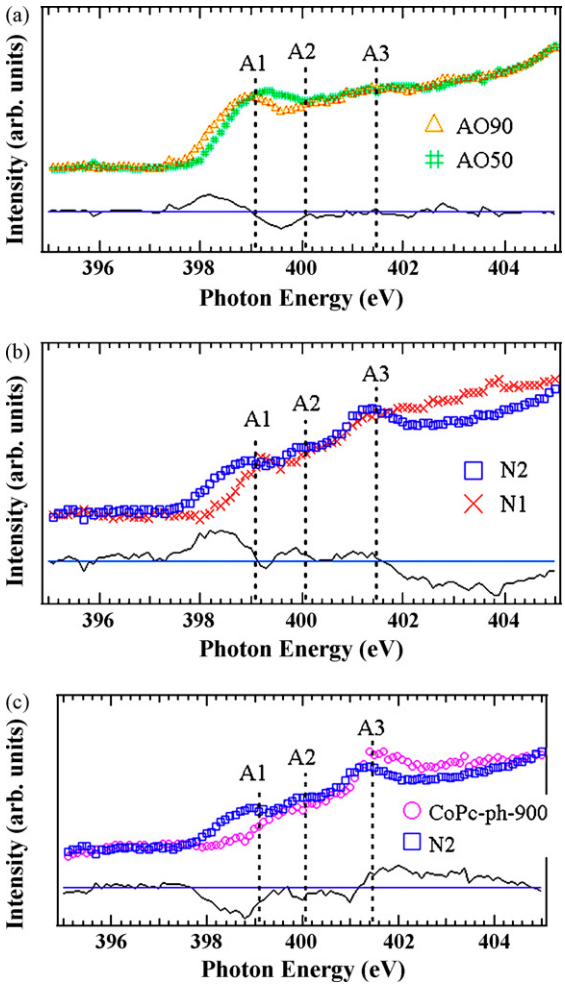

Fig. 5. XAS differences in the π^* region for (a) AO90 and AO50, (b) N2 and N1, and (c) CoPc-ph-900 and N2. In Fig. 5(a), (b) and (c), black lines represent the difference of absorption intensity calculated by subtracting AO50 from AO90, N1 from N2, and N2 from CoPc-ph-900, respectively, and blue lines represent the zero line of the difference. (For interpretation of the references to color in this figure legend, the reader is referred to the web version of the article.)

exhibit a higher ORR activity than those bonded to pyridine-like nitrogen [24]. Although it is quite difficult to distinguish graphite-like nitrogen at the zigzag edge from that in the graphene sheet by XAS, the results of such a simulation are qualitatively in good agreement with our XAS results.

4. Conclusions

We prepared three types of carbon alloy cathode catalyst for the PEFC and measured ORR activity and soft X-ray absorption spectra to determine the role of nitrogen in the catalytic reaction in carbon alloys. The obtained results indicate that samples with a larger amount of graphite-like nitrogen exhibit a higher ORR activity than those with a larger amount of pyridine-like nitrogen. Thus, effective doping with graphite-like nitrogen should be a practical guideline for the synthesis of active carbon alloy catalysts.

Acknowledgment

This work was performed under Project 07003613-0 at the New Energy and Industrial Technology Development Organization (NEDO).

References

[1] P. Costamagna, S. Srinivasan, J. Power Sources 102 (2001) 242–252.
[2] H. Zhong, H. Zhang, G. Liu, Y. Liang, J. Hu, B. Yi, Electrochem. Commun. 8 (2006) 707–712.
[3] X. Yu, S. Ye, J. Power Sources 172 (2007) 133–144.
[4] V.R. Stamenkovic, B.S. Mun, M. Arenz, K.J.J. Mayrhofer, C.A. Lucas, G. Wang, P.N. Ross, N.M. Markovic, Nat. Mater. 6 (2007) 241–247.
[5] R. Jasinski, J. Electrochem. Soc. 112 (1964) 526–528.
[6] V.S. Bagotzky, M.R. Tarasevich, K.A. Radyushkina, O.A. Levina, S.I. Andrusyova, J. Power Sources 2 (1977) 233–240.
[7] R. Bashyam, P. Zelenay, Nature 443 (2006) 63–66.
[8] A. Ishihara, Y. Shibata, S. Mitsushima, K. Ota, J. Electrochem. Soc. 155 (2008) B400–B406.
[9] J. Ozaki, N. Kimura, T. Anahara, A. Oya, Carbon 45 (2007) 1847–1853.
[10] J. Ozaki, T. Anahara, N. Kimura, A. Oya, Carbon 44 (2006) 3358–3361.
[11] J. Ozaki, S. Tanifuji, N. Kimura, A. Furuichi, A. Oya, Carbon 44 (2006) 1324–1326.
[12] S. Maldonado, K.J. Stevenson, J. Phys. Chem. B 108 (2004) 11375–11383.
[13] P.H. Matter, S.O. Umit, Catal. Lett. 109 (2006) 115–123.
[14] S. Maldonado, K.J. Stevenson, J. Phys. Chem. B 109 (2005) 4707–4716.
[15] Y. Tanabe, E. Yasuda, Carbon 38 (2000) 329–334.
[16] Y. Shao, J. Sui, G. Yin, Y. Gao, Appl. Catal. B: Environ. 79 (2008) 89–99.
[17] H. Niwa, K. Horiba, Y. Harada, M. Oshima, S. Ueda, Y. Yamashita, H. Yoshikawa, K. Kobayashi, T. Ikeda, K. Terakura, J. Ozaki, S. Miyata, submitted for publication.
[18] M.W. Schmidt, K.K. Baldridge, J.A. Boatz, S.T. Elbert, M.S. Gordon, J.H. Jensen, S. Koseki, N. Matsunaga, K.A. Nguyen, S.J. Su, T.L. Windus, M. Dupuis, J.A. Montgomery, J. Comput. Chem. 14 (1993) 1347–1363.
[19] J.M. Ripalda, E. Román, N. Díaz, L. Galán, I. Montero, G. Comelli, A. Baraldi, S. Lizzit, A. Goldoni, G. Paolucci, Phys. Rev. B 60 (1999) R3705–R3708.
[20] J. Stöhr, NEXAFS Spectroscopy, Springer, Berlin, 1992, pp. 110–111.
[21] N. Mubumbila, B. Bouchet-Fabre, C. Godon, C. Marhic, B. Angleraud, P.-Y. Tessier, T. Minea, Diamond Relat. Mater. 13 (2004) 1433–1436.
[22] R. Gago, I. Jiménez, J. Neidhardt, B. Abendroth, I. Caretti, L. Hultman, W. Möller, Phys. Rev. B 71 (2005) 125414.
[23] N. Hellgren, J. Guo, Y. Luo, C. Såthe, A. Agui, S. Kashtanov, J. Nordgren, H. Ågren, J. Sundgren, Thin Solid Films 471 (2005) 19–34.
[24] T. Ikeda, M. Boero, S. Huang, K. Terakura, M. Oshima, J. Ozaki, J. Phys. Chem. C 112 (2008) 14706–14709.